The Effect of Bacteriochlorophyll g Oxidation on Energy and Electron Transfer in Reaction Centers from Heliobacterium modesticaldum

ARTICLE *in* THE JOURNAL OF PHYSICAL CHEMISTRY B · JUNE 2015

Impact Factor: 3.3 · DOI: 10.1021/acs.jpcb.5b03339 · Source: PubMed

THE JOURNAL OF PHYSICAL CHEMISTRY B

Article

pubs.acs.org/JPCB

The Effect of Bacteriochlorophyll *g* Oxidation on Energy and Electron Transfer in Reaction Centers from *Heliobacterium modesticaldum*

Bryan Ferlez,[†,%] Weibing Dong,[†,%] Reza Siavashi,[∥] Kevin Redding,[#] Harvey J. M. Hou,*[,§] John. H. Golbeck,*[,†,‡] and Art van der Est*[,∥,⊥]

[†]Department of Biochemistry and Molecular Biology and [‡]Department of Chemistry, The Pennsylvania State University, University Park, Pennsylvania 16802, United States

[§]Department of Physical Sciences, Alabama State University, Montgomery, Alabama 36104, United States

[∥]Department of Physics and [⊥]Department of Chemistry, Brock University, 500 Glenridge Avenue, St. Catharines, ON Canada L2S 3A1

[#]Department of Chemistry & Biochemistry, Arizona State University, Tempe, Arizona 85287, United States

ABSTRACT: The heliobacteria are a family of strictly anaerobic, Gram-positive, photoheterotrophs in the Firmicutes. They make use of a homodimeric type I reaction center (RC) that contains ~20 antenna bacteriochlorophyll (BChl) *g* molecules, a special pair of BChl *g*′ molecules (P_{800}), two 8^1-OH-Chl a_F molecules (A_0), a [4Fe−4S] iron−sulfur cluster (F_X), and a carotenoid (4,4′-diaponeurosporene). It is known that in the presence of light and oxygen BChl *g* is converted to a species with an absorption spectrum identical to that of Chl *a*. Here, we show that main product of the conversion is 8^1-OH-Chl a_F. Smaller amounts of two other oxidized Chl a_F species are also produced. In the presence of light and oxygen, the kinetics of the conversion are monophasic and temperature dependent, with an activation energy of 66 ± 2 kJ mol^{-1}. In the presence of oxygen in the dark, the conversion occurs in two temperature-dependent kinetic phases: a slow phase followed by a fast phase with an activation energy of 53 ± 1 kJ mol^{-1}. The loss of BChl *g*′ occurs at the same rate as the loss of Bchl *g*; hence, the special pair converts at the same rate as the antenna Chl's. However, the loss of P_{800} photooxidiation and flavodoxin reduction is not linear with the loss of BChl *g*. In anaerobic RCs, the charge recombination between P_{800}^+ and F_X^- at 80 K is monophasic with a lifetime of 4.2 ms, but after exposure to oxygen, an additional phase with a lifetime of 0.3 ms is observed. Transient EPR data show that the line width of P_{800}^+ increases as BChl *g* is converted to Chl a_F and the rate of electron transfer from A_0 to F_X, as estimated from the net polarization generated by singlet−triplet mixing during the lifetime of $P_{800}^+A_0^-$, is unchanged. The transient EPR data also show that conversion of the BChl *g* results in increased formation of triplet states of both BChl *g* and Chl a_F. The nonlinear loss of P_{800} photooxidiation and flavodoxin reduction, the biphasic backreaction kinetics, and the increased EPR line width of P_{800}^+ are all consistent with a model in which the BChl *g*′/BChl *g*′ and BChl *g*′/Chl a_F′ special pairs are functional but the Chl a_F′/Chl a_F′ special pair is not.

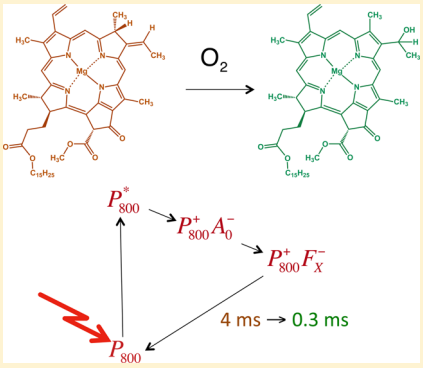

1. INTRODUCTION

Heliobacteria are anoxygenic phototrophic bacteria that contain a homodimeric type I reaction center (RC),[1] but unlike green sulfur bacteria or chloracidobacteria, they do not contain chlorosomes or antenna complexes and rely solely on pigments bound to the RC for light harvesting.[2] They are also the only photosynthetic organism that makes use of bacteriochlorophyll (BChl) *g*,[3] which allows them to harvest near-infrared light in their native soil environment.[1] Compared to photosystem I (PS I) of cyanobacteria and plants, the heliobacterial reaction center (HbRC) contains fewer pigments and protein subunits and, as a result, it is an ideal model for the study of a simple, prototypical homodimeric RC.[2] In the HbRC, 20 BChl *g* molecules[4,5] function as an antenna along with the carotenoid 4,4′-diaponeurosporene.[6,7] The primary electron donor, P_{800}, is a special pair of BChl *g*′ molecules (the 13^2 epimer of Chl *g*),[5,8] while the primary acceptor, A_0, is 8^1-OH-chlorophyll a_F (where the subscript F stands for farnesyl).[9] Unlike PS I, the HbRC does not contain a tightly bound dicluster ferredoxin as a subunit.[10] Instead, the F_X cluster functions as the terminal acceptor, donating electrons to a variety of soluble redox partners, including the loosely bound dicluster ferredoxins PshB1 and PshB2.[11] The HbRC also contains menaquinone,[12] but its function remains unclear.[6] Time-resolved optical and EPR data show that electron transfer between A_0 and the iron sulfur cluster F_X occurs with a lifetime of ~600 ps[13−17] and there is no evidence from kinetic lifetimes for an intermediate between these two acceptors.[17−19] However, EPR signals assigned to a photoreduced quinone radical have been reported

Special Issue: Wolfgang Lubitz Festschrift

Received: April 8, 2015
Revised: May 20, 2015

DOI: 10.1021/acs.jpcb.5b03339
J. Phys. Chem. B XXXX, XXX, XXX−XXX

in samples that have been treated with dithionite to reduce F_X.[20−22]

Heliobacteria grow only under strictly anaerobic conditions, and when exposed to air, the major photosynthetic pigment, BChl *g*, is oxidized to a species with an absorbance spectrum identical to that of Chl *a*[23,24] (Scheme 1). In cells and isolated membranes, the two Soret transitions and Q_X and Q_Y bands of BChl *g* occur at 368, 409, 575, and 788 nm, respectively.[25,26] On exposure to air and light, the Q_Y transition shifts to 670 nm, resulting in a color change from brown to emerald green.[23]

Scheme 1. Molecular Structure of (A) BChl *g*, (B) Chl a_F, and (C) 8^1-OH-Chl a_F according to the IUPAC Numbering System

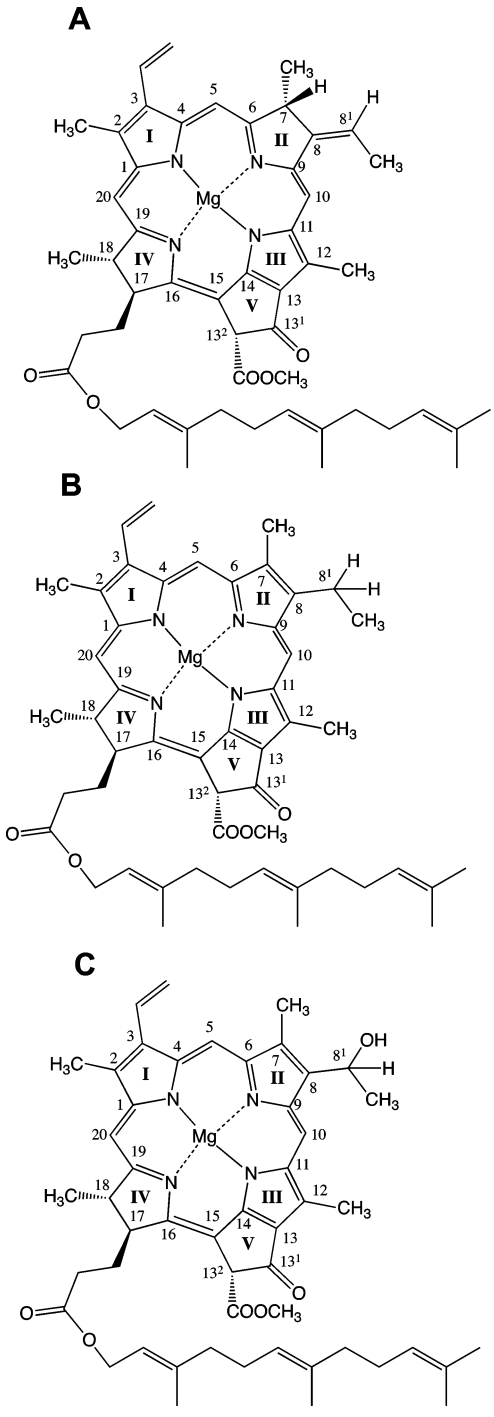

This shift can be used to conveniently monitor the conversion by optical absorption spectroscopy.[24]

The chemical structure of the oxidation product (or products) and the effect of this conversion on the function of HbRCs have not been adequately investigated. Recently, an NMR study[27] demonstrated that 80% conversion of BChl *g* does not impair the appearance of dynamic nuclear polarization (photo-CIDNP) resonances, indicating that light-induced charge separation takes place. This system therefore presents a unique opportunity to investigate the influence of chlorophyll energetics on the kinetics and quantum yield of energy and electron transfer, since the alteration of the chlorophyll does not require any mutagenesis or cofactor exchange. Moreover, the conversion is not expected to significantly perturb the arrangement of the chlorophylls and their binding sites within the protein matrix while still causing a large change in the energetics, as evidenced by the shift of nearly 100 nm in the Q_y absorbance transition. However, before the effect of the conversion on the function of the RC can be studied in detail, the conversion itself must be better understood. Here, we report a systematic study of the conversion of BChl *g* and a first investigation of its effect on energy and electron transfer in homodimeric type I RCs isolated from *Heliobacterium modesticaldum*.

2. EXPERIMENTAL SECTION

2.1. Growth and Isolation of HbRC Cores. Cultures of *Heliobacterium modesticaldum* were generously provided by Prof. Mike Madigan (Southern Illinios University, Carbondale, IL). Liquid cultures of *H. modesticaldum* were grown anaerobically in PYE media.[28] Resazurin, an oxygen reporter dye, was added to a final concentration of 0.001%. All manipulations were performed under anoxic conditions. Cells grown to late-exponential phase were harvested at 10 000*g* for 30 min and resuspended in 50 mM MOPS buffer (pH 7.0). Whole cells were lysed by sonication, and unbroken whole cells were removed by centrifugation at 10 000*g*. The dark brown supernatant, which contains the membranes, was pelleted by centrifugation at 200 000*g* and solubilized with 1% *n*-dodecy-*β*-D-maltopyranoside (DDM) for 1 h. Unsolubilized membranes were removed by centrifugation at 200 000*g* for 30 min. The supernatant was passed over a diethylaminoethyl (DEAE) cellulose ion-exchange column equilibrated in 50 mM MOPS containing 0.02% DDM (pH 7.0). This removes the PshBI and PshBII polypeptides that contain the F_A and F_B clusters. The flowthrough contained the HbRC cores in which F_X is the terminal electron acceptor.[11] The HbRC cores were concentrated by ultrafiltration and stored in liquid nitrogen until use.

2.2. UV−Visible Absorption Spectroscopy. UV−visible absorption spectroscopy was carried out using a Varian Cary 50 spectrophotometer. All spectra were corrected for background and offset effects. The spectra of HbRC cores were measured in 3 mL quartz cuvettes with a 10 mm path length at an optical transmittance of 0.8 OD at 788 nm. A 25 W tungsten lamp coupled with a fiber optic cable (diameter = 1 cm) was used to drive the photo-oxidation of BChl *g* at temperatures ranging from 297 to 319 K, and spectra were recorded every 10 min.

2.3. HPLC-Mass Spectrometry of RC Pigments. High-performance liquid chromatography (HPLC) with detection by mass spectrometry (LC-MS) was conducted on an Agilent Technologies (Santa Clara, CA) 1200 system coupled to an Agilent Technologies 6410 QQQ mass spectrometer. The

DOI: 10.1021/acs.jpcb.5b03339
J. Phys. Chem. B XXXX, XXX, XXX−XXX

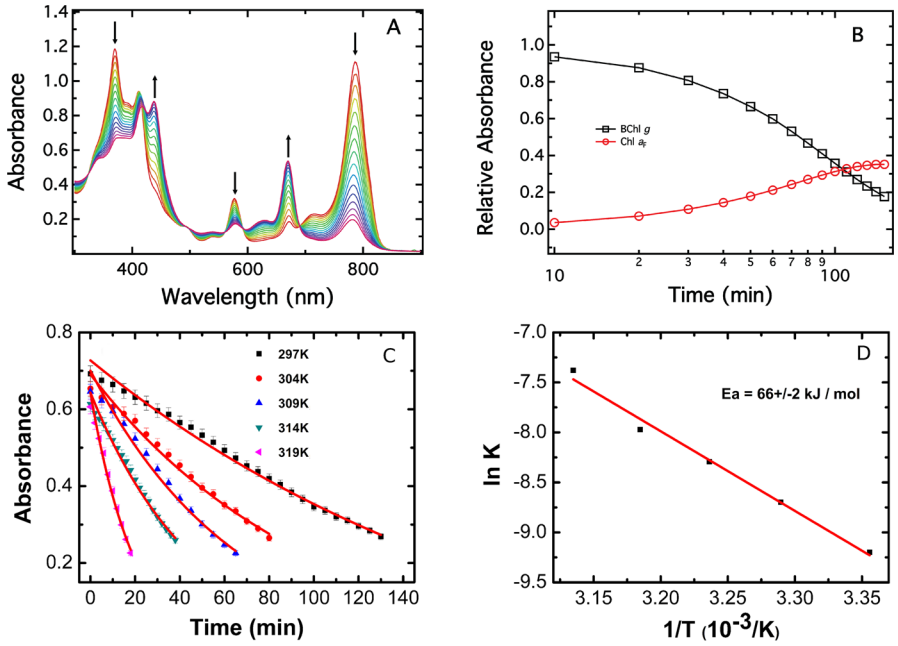

Figure 1. Effect of light and O_2 on the conversion of BChl *g* to a Chl a_F in isolated heliobacterial RCs at 298 K. The light intensity at the surface of the cuvette was 40 μmol m^{-2} s^{-1}, and the dissolved O_2 concentration of the solution was 8.3 mg L^{-1} (air saturated water at 298 K, corrected for barometric pressure). (a) Spectra at 10 min intervals. (b) Time course of the decline in the amplitude of the Q_y peak of BChl *g* ($A_{788}/A_{788}(t = 0)$, black squares) and the subsequent rise in the amplitude of the Chl a_F Q_y peak ($A_{670} - A_{670}(t = 0)$, red circles). (c) Decline in the amplitude of the Q_y peak of BChl *g* at various temperatures. The data was fit with an exponential decay function to obtain rate constants of 1.01 × 10^{-4} s^{-1} (297 K), 1.67 × 10^{-4} s^{-1} (304 K), 2.5 × 10^{-4} s^{-1} (309 K), 3.45 × 10^{-4} s^{-1} (314 K), and 6.25 × 10^{-4} s^{-1} (319 K). (d) Arrhenius plot for the first-order rate constant of the conversion of BChl *g* to Chl a_F.

system was operated with the associated MassHunter software package, which was also used for data collection and analysis.

Pigments were extracted from HbRC preparations (3.2 mM BChl *g*) in acetone/0.1% formic acid (pH 2.6) and were separated on an Agilent Technologies Zorbax Extend-C18 RRHT column (4.6 mm × 50 mm, 1.8 μm particle size) equilibrated in 100% solvent A (74:6:1 acetonitrile:methanol:-formic acid, pH 2.6). After 2 min at 100% solvent A, a gradient of 0−100% solvent B (5:1 methanol:acetonitrile) was applied from 2 to 4.5 min and maintained at 100% solvent B from 4.5 to 9 min before returning to 0% solvent B from 9 to 10 min. A flow rate of 0.5 mL/min was maintained throughout the chromatographic procedure. The column was allowed to re-equilibrate for 3 min under initial conditions before subsequent sample injections. Prior to quantification of the relative BChl *g* and BChl *g*′ content, the HPLC traces were normalized to the content of the carotenoid 4,4′-diaponeurosporene (*m*/*z* 402.5), which elutes at approximately 6.4 min under these conditions.

BChl *g* and Chl a_F derivatives were detected by MS2 selected-ion monitoring at *m*/*z* ratios of 811.5, 819.5, 835.5, and 851.5. Detection of analytes was performed by selected ion monitoring (SIM) using electrospray ionization in positive mode (ESI^+) with a nitrogen gas temperature of 350 °C and a flow rate of 9.0 L/min, a nebulizer pressure of 40 PSI, and a capillary voltage of 4000 V. The optimal fragmentor voltage for BChl *g* and Chl a_F derivatives was determined to be 90 V, while the optimal fragmentor voltage for the 4,4′-diaponeurosporene was determined to be 150 V.

UV−visible absorbances were collected at 752 (20), 662 (20), 410 (20), 464 (20), and 280 (8) nm (bandwidth denoted in parentheses). UV−visible spectra were collected from 260 to 900 nm in 2 nm steps every 0.5 s using the associated diode array detector.

2.4. Flavodoxin Reduction Assay. Dilute HbRCs at 70 μM [BChl *g*] were illuminated with a xenon lamp at an intensity of 224 μmol of photons m^{-2} s^{-1} to convert BChl *g* to Chl *a*. At each time point, a sample was removed, sealed, and purged with argon gas at 6 psi for 15 min to remove O_2 from the solution. Flavodoxin reduction assays were then carried out as described in detail by Romberger and Golbeck.[11] Briefly, the change in the absorbance of flavodoxin was monitored at 467 nm while the sample was illuminated using white light. The rate of flavodoxin reduction was determined by a linear fit to the absorbance change over the first 1−2 s of illumination. Each flavodoxin measurement is the average of three data collections. The percent of BChl *g* converted was determined by comparison of the Q_y band of BChl *g* as a function of light and O_2 exposure.

2.5. P_{800} Photobleaching and Time Resolved Optical Spectroscopy. P_{800} photobleaching was measured on a JTS-10 pump probe spectrometer (BioLogic) using a continuous orange ring LED actinic light source (λ_{max} = 640 nm) and a pulsed probe beam provided by an 810 nm LED. To monitor photobleaching at 800 nm, an interference filter was placed between the probe beam and the sample. HbRC samples were prepared by dilution with 50 mM MOPS pH 7.0 with 0.02% DDM and 10 mM sodium ascorbate with a final [BChl *g*] of ∼400 μM.

To determine the differential absorption spectrum of the RC following conversion of BChl *g* to Chl a_F, the amplitude of the light induced absorbance change of an anaerobic and 89% converted sample was measured 10 μs after a saturating laser flash provided by a frequency doubled Nd:YAG laser (SpectraPhysics). Using light from a tungsten lamp passed through a monochromator as well as an interference filter, absorbance changes were measured every 10−20 nm from 509

DOI: 10.1021/acs.jpcb.5b03339
J. Phys. Chem. B XXXX, XXX, XXX−XXX

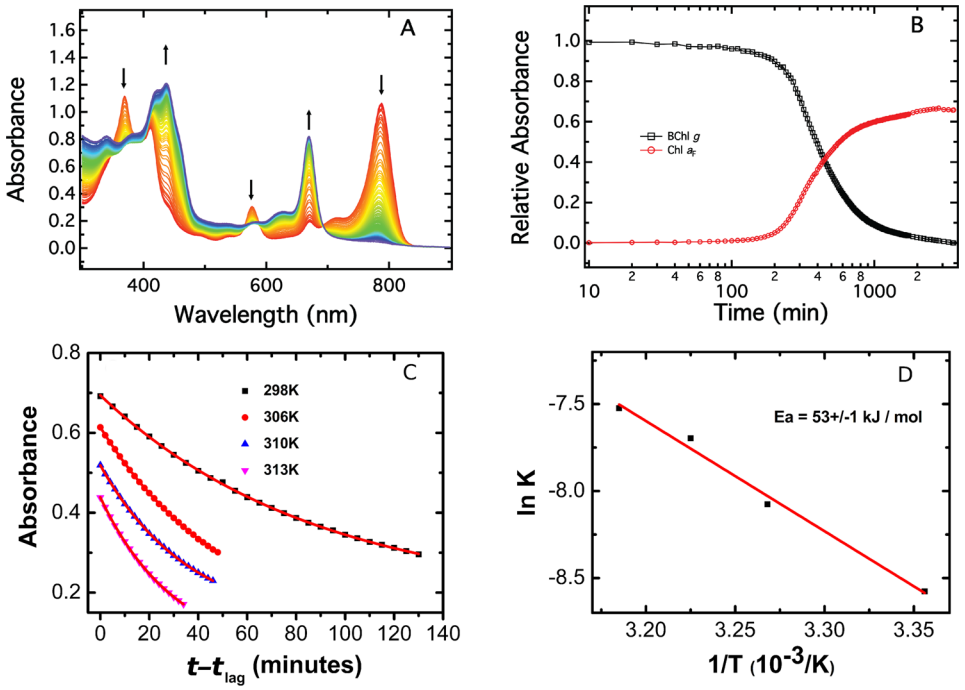

Figure 2. Effect of O_2 on the conversion of BChl *g* to Chl *a* in isolated HbRCs at 298 K in the dark. (a) Representative spectra taken over the course of 60 h. (b) Time course of the decline in the amplitude of the Q_y peak of BChl *g* ($A_{788}/A_{788}(t = 0)$, black squares) and the subsequent rise in the amplitude of the Chl a_F Q_y peak ($A_{670} - A_{670}(t = 0)$, red circles). (c) Fast phase of the decline in the amplitude of the Q_y peak of BChl *g* at various temperatures. For each temperature, the zero point on the time axis was chosen as the time at which the transition from the initial lag phase to the fast phase was deemed to be complete (Table 1). The initial absorbance of the samples was 0.85. The data were fit with an exponential decay function to obtain rate constants of 1.885×10^{-4} s^{-1} (298 K), 3.109×10^{-4} s^{-1} (306 K), 4.543×10^{-4} s^{-1} (310 K), and 5.403×10^{-4} s^{-1} (314 K). (d) Arrhenius plot for the first-order rate constant of the conversion of BChl *g* to Chl a_F.

to 910 nm. Each point is the average delta absorbance from 64 collections. The sample composition was 10 μM BChl *g* and 10 mM sodium ascorbate in 50 mM MOPS pH 7.0 with 0.02% DDM.

2.6. Transient EPR Experiments. Time/field transient EPR data sets were collected using a modified Bruker ER 200D-SRC spectrometer with either an ER 041 X-MR X-band or an ER 051 QR Q-band microwave bridge. For the X-band data sets, a Bruker Flexline ER 4118 X-MD-5W1 dielectric resonator was used. A Bruker ER 5106 QT-W cylindrical resonator was used for the Q-band experiments. Light excitation was achieved using a Continuum Surelite Nd:YAG laser operating at 10 Hz and a wavelength of 532 nm and 4.0 mJ/pulse. The temperature was controlled using an Oxford Instruments CF935 gas flow cryostat. The spin-polarized transient EPR signals of the chlorophyll triplet states and radical pair $P_{800}^{+}F_X^{-}$ were collected in direct-detection mode with a home-built broadband amplifier (bandwidth >500 MHz). For measurements of the lifetime of P_{800}^{+}, the signal was collected using lock-in detection and a Bruker ER032 signal channel. In both cases, the signals were digitized using a LeCroy LT322 500 MHz digital oscilloscope and saved on a computer for analysis. For the EPR experiments, HbRCs were exposed to air in the dark at ambient temperature for varying amounts of time up to 12 h at which point dissolved oxygen was removed by purging each sample with argon gas at 6 psi for 15 min. Samples were then moved to an anaerobic chamber (Coy Laboratories), and the sample was transferred to EPR tubes and frozen in the dark with liquid nitrogen.

3. RESULTS

3.1. Absorption Changes in the HbRC under Illumination with Dioxygen as Oxidant. In an earlier study,[5] we made the unexpected discovery that purified HbRCs isolated from *Heliobacterium modesticaldum* were more stable to O_2 than was previously thought. Thus, it is of interest to better understand the effect of light, oxygen, and temperature on the conversion of BChl *g* to Chl a_F. The absorption spectra of RC cores in 50 mM MOPS buffer (pH 7.0) at 298 K in the presence of O_2 and light are shown at 10 min intervals of illumination in Figure 1A. Over the course of 2 h, the characteristic peaks of BChl *g* at 788, 575, and 368 nm decline, while the characteristic peaks of Chl a_F at 670 and 438 nm increase. During this time, the appearance of the solution changes from brown to emerald green. The presence of multiple isosbestic points, especially prominent at 695, 595, and 480 nm, indicates that the conversion occurs without the accumulation of an apparent intermediate. The decline of the intensity of the 788 nm peak from BChl *g* and the rise of the intensity of the 670 nm peak from Chl a_F are plotted against time on a logarithmic scale in Figure 1B. (For the 788 nm peak, the absorbance relative to the initial intensity is plotted. For the 670 nm peak, the absolute absorbance increase is shown.) The loss of BChl *g* is exponential with time and mirrors the increase in Chl a_F. At room temperature (297 K), 2 h are required for 63% of BChl *g* to be converted to Chl a_F, which corresponds to a rate constant of 1.01×10^{-4} s^{-1}. The loss in the amplitude of BChl *g* at 788 nm, measured at five temperatures, is shown in Figure 1C, and an Arrhenius plot of the rate constants (Figure 1D) yields an activation energy of 66 ± 2 kJ mol^{-1} for the light-mediated conversion of BChl *g* to Chl a_F in the presence of O_2.

DOI: 10.1021/acs.jpcb.5b03339
J. Phys. Chem. B XXXX, XXX, XXX−XXX

3.2. Absorption Changes in the HbRC in Darkness with Dioxygen as Oxidant. The absorption spectra of HbRCs incubated in the dark at 298 K in the presence of O_2 are shown in Figure 2A. Similar to the study carried out in light, the characteristic peaks of BChl *g* at 788, 575, and 368 nm decreased, while the characteristic peaks of Chl a_F at 670 and 438 nm increased and the presence of the same isosbestic points indicates that no detectable intermediate accumulates during the conversion. The decline of the intensity of the 788 nm peak from BChl *g* and the rise of the intensity of the Chl a_F at 670 nm are plotted against time on a logarithmic scale in Figure 2B. The conversion of BChl *g* to Chl a_F can be seen to occur in two distinct phases. Over the first 3 h, the 788 nm peak decreases slowly from 1.07 OD to 0.98 OD, during which time only 8% of BChl *g* is converted to Chl a_F. At the 3 h point, a seemingly abrupt transition occurs, and the absorbance decreases rapidly from 0.98 OD to 0.44 OD over the course of 6 h, during which time approximately 45% of BChl *g* is converted to Chl a_F. The absorbance decay during the initial slow phase could not be fitted easily with a simple kinetic model, but the fast decay is exponential and the activation energy of this phase was determined. Figure 2C shows the temperature dependence of the fast phase of the 788 nm absorbance loss. For each temperature, the point at which the transition from the slow to fast phase was deemed to be complete (Table 1) was chosen as the zero point on the time axis for the data in Figure 2C. The Arrhenius plot of the rate constants (Figure 2D) gives an activation energy of 53 ± 1 kJ mol^{-1} for the fast phase in the conversion of BChl *g* to Chl a_F in the dark.

Table 1. Duration of the Slow Kinetic Phase of BChl *g* Oxidation in the Dark as a Function of Temperature

temperature (K)	duration (min)
273	>1500
282	720
298	245
306	110
310	66
313	54

3.3. Effect of Vitamin K3 on the O_2-Mediated Conversion of BChl *g* to Chl *a* in the Dark. Menadione (vitamin K3) significantly retards the rate of the dark O_2-mediated conversion of BChl *g* to Chl *a*. At an equimolar ratio of menadione to HbRC, the absorbance at the 788 nm peak of BChl *g* decreases from 0.75 OD to 0.65 OD after 20 h of exposure to O_2. This loss of absorbance corresponds to a conversion of only 13% of the bulk BChl *g* pigment, which is significantly less than the 49% conversion observed in a sample of identical HbRCs exposed to O_2 in the absence of menadione. The conversion of BChl *g* to Chl a_F could be further arrested to the point that no conversion could be detected over 20 h by increasing the molar ratio of menadione to RC to 30:1 (data not shown).

3.4. HPLC-Mass Spectrometry of Pigments during Dark Dioxygen Exposure. The multiphasic kinetics of the conversion in the dark suggests that exposure to O_2 does not just lead to simple isomerization of BChl *g* to Chl a_F and it is possible that multiple oxidation products are formed as observed previously for the conversion in diethyl ether and other solvents.[24] Hence, we performed an HPLC-MS analysis to determine which species are present in the samples. This analysis also allows the rate of conversion of the BChl *g*′ pigments, which constitute the P_{800} special pair, to be compared to that of the BChl *g* cofactors. The total pigment content extracted from HbRCs that had been exposed to O_2 for varying times in the dark corroborates the conversion of BChl *g* to Chl a_F shown above in the UV−visible experiments. Consistent with previously published results,[5] four major peaks are observed in the control sample prior to exposure to O_2 (Figure 3A, peaks 2, 4, 5, and 8), and these can be assigned to 8^1-OH-Chl a_F, BChl *g*, BChl *g*′, and 4,4′-diaponeurosporene, respectively (Figure 3B). Small amounts of residual O_2 in the sample or extraction buffer (0.1% formic acid/acetone) likely lead to the accumulation of some isomerized BChl *g* (Figure 3A, peak 7 - Chl a_F), consistent with the acid catalyzed mechanism proposed by Kobayashi et al.[24] The relative amount of this species is independent of the loss of BChl *g* and therefore is not related to the dark conversion that occurs prior to extraction. After 6 h of exposure to O_2, the content of 8^1-OH-Chl a_F (peak 2) increases and three new peaks are observed (Figure 3A, peaks 1, 3, and 6). Peak 1 grows in as a distinct shoulder on the leading edge of peak 2 and has an absorption spectrum and mass to charge ratio (*m*/*z*) that suggests a Chl a_F species with the addition of two hydroxyl groups. The absorption spectrum and *m*/*z* of peak 3 suggest it is another Chl a_F derivative with the addition of a single oxygen atom. Hence, the conversion product of BChl *g* after exposure to O_2 is 8^1-OH-Chl a_F with an additional small amount of what is tentatively identified as 8^1-geminal-diol-Chl a_F and its dehydration product, 8^1-keto-Chl a_F. All three oxidation products of BChl *g* will be collectively termed Chl a_{ox} in this paper. Peak 6 also has an absorption spectrum and *m*/*z* value that is similar to peak 1 which suggests it is also a Chl *a* derivative; however, its retention time is unexpectedly longer (ca. 5.5 min) and further study is required to determine its origin.

The total BChl *g*′ content (Figure 3A, peak 5) of the sample can be seen to decrease linearly with the loss of BChl *g* (Figure 3C). When the integrated area of this peak is plotted as a function of the total BChl *g* converted, the data can be fit with a straight line with a slope of −1.1 and an r^2 value of 0.99. Thus, the special pair BChl *g*′ molecules are nearly equally susceptible to oxidative conversion as the antenna BChl *g* molecules.

3.5. Flavodoxin Reduction Rates and Transient Optical Spectroscopy during Conversion. The steady-state rates of flavodoxin reduction were compared to the extent of photobleaching of the primary donor P_{800} at various points in the conversion of BChl *g* to Chl a_{ox}. The rates of flavodoxin reduction were determined from the time dependence of the associated absorbance change at 467 nm, while the photobleaching of the primary donor was monitored at 800 nm. The flavodoxin reduction reflects the rate at which the HbRCs are able to withdraw electrons from the soluble donor 1-methoxy-5-methylphenazinium methyl sulfate (PMS) and transfer them to the soluble acceptor flavodoxin, whereas the photobleaching of P_{800} is a measure of the yield of charge separation between P_{800} and F_X. As shown in Figure 4A, both of these measures of the activity of the HbRCs show the same dependence on the degree of BChl *g* conversion. To distinguish between inefficient energy transfer and loss of electron transfer, the dependence of the flavodoxin reduction on the light intensity was studied. As the light intensity is increased, the rate of flavodoxin reduction follows a saturation curve. The efficiency of the energy transfer

DOI: 10.1021/acs.jpcb.5b03339
J. Phys. Chem. B XXXX, XXX, XXX−XXX

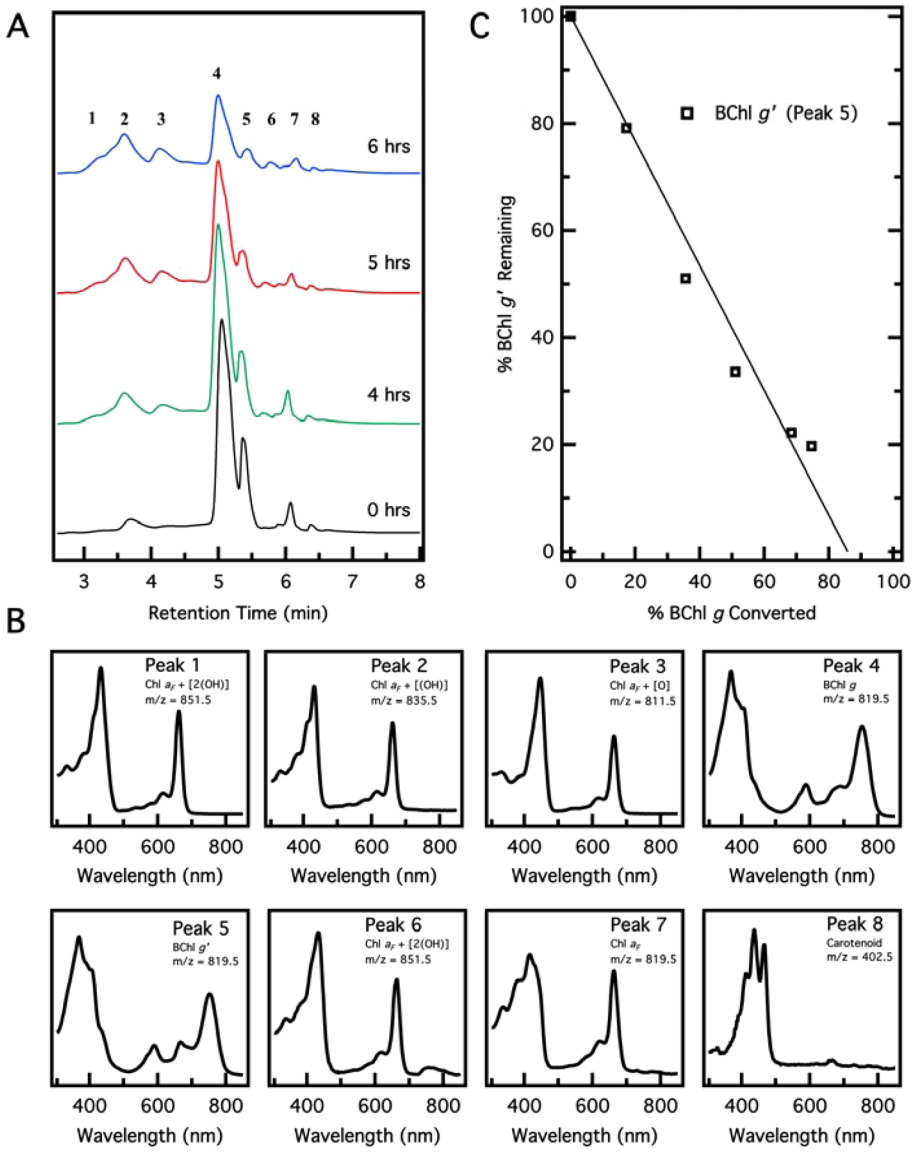

Figure 3. HPLC and mass spectrometry analysis of RC pigments during O_2 exposure. (a) HPLC retention traces of RC pigments monitored at 410 nm during exposure to O_2. (b) Plot of the linear loss of BChl *g*′ as a function of total BChl *g* conversion. All HPLC spectra were normalized by carotenoid content (peak 8). (c) UV−visible spectra of each of the eight peaks observed during O_2 mediated conversion. Assignments of pigments were determined by both the *m*/*z* values and UV−visible absorbance spectrum for each peak. Peak 7 represents the acid mediated isomerization of BChl *g* under acidic conditions due to residual oxygen in either the extraction solution (0.1% formic acid/acetone) or the RC prep sample.

is reflected in the amount of light needed to reach saturation, and the maximum rate of flavodoxin reduction reflects the electron transfer efficiency. Impairment of the energy transfer results in more light being required to reach saturation, and lower electron transfer efficiency results in a lower rate at saturation. Light saturation curves were measured for the 0 and 70% BChl *g* converted samples (Figure 4B). The half-saturation light intensity for the 70% converted sample (39 mW) is ca. 4 times greater than that for the 0% converted sample (11 mW), indicating impaired efficiency of energy transfer among the antenna pigments (see section 3.8 below). Nevertheless, the amount of reduced flavodoxin saturates at a lower value for the 70% converted sample (0.099 ΔAbs_{467nm}) than the 0% converted sample (0.135 ΔAbs_{467nm}), showing that, at saturation, activity is lost due to loss of charge separation.

Figure 4A shows that the dependence of the flavodoxin reduction and amplitude of P_{800} bleaching on the degree of BChl *g* (or BChl *g*′) conversion is nonlinear. For example, at 30% BChl *g* conversion, there is no appreciable loss of flavodoxin reduction and P_{800}^+ formation. This behavior is not consistent with a model in which conversion of one of the special pair BChl *g*′ molecules is sufficient to inactivate the HbRC. The observed dependence on the degree of conversion can be explained in the following manner. The distribution of possible pigment combinations in the primary donor, (BChl *g*′/BChl *g*′), (Chl *a*′/BChl *g*′), or (Chl *a*′/Chl *a*′), can be determined from the degree of conversion of BChl *g*′. Since the rates of conversion of BChl *g* and BChl *g*′ are equal (Figure 3C), the overall degree of conversion of BChl *g* can be used. The population of each of the three possible forms of the primary donor is given by the product of the fractions of each of the pigments in the RC. As shown in Figure 4C, the BChl *g*′/BChl *g*′ containing special pair is predicted to decrease with conversion (brown line), while the (Chl *a*′/Chl *a*′) containing

DOI: 10.1021/acs.jpcb.5b03339
J. Phys. Chem. B XXXX, XXX, XXX−XXX

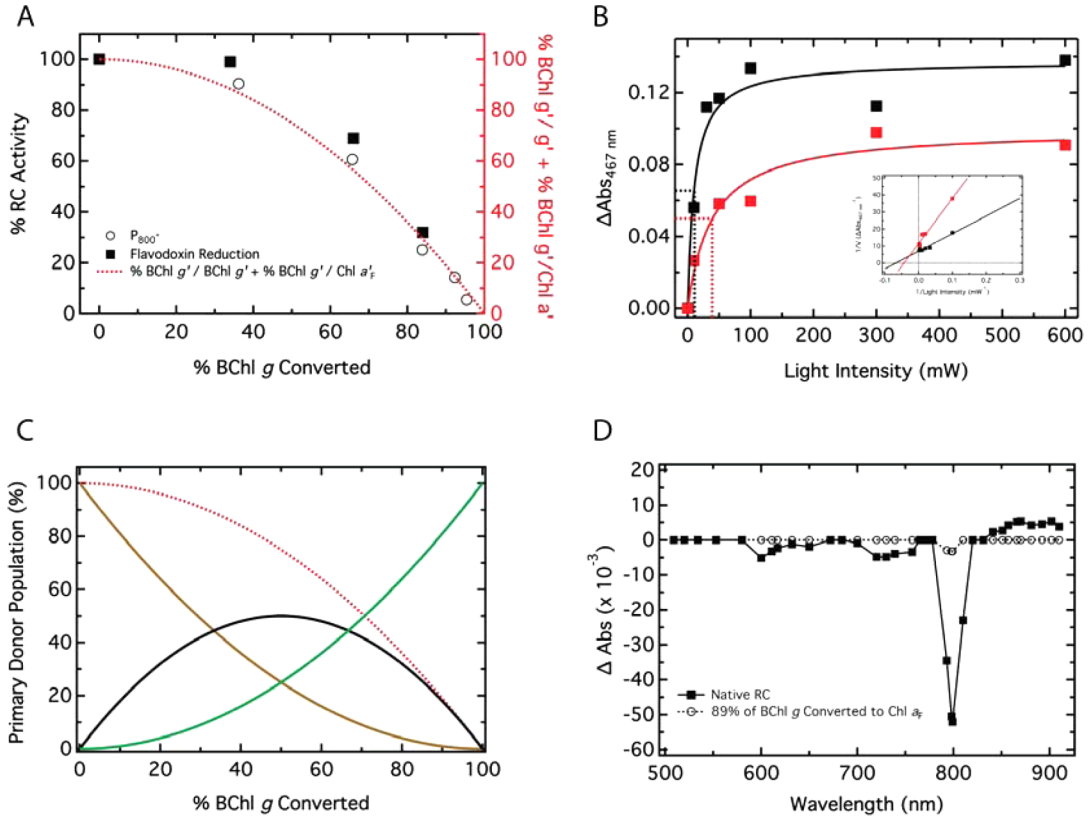

Figure 4. P_{800}^{+} photoxidation and flavodoxin reduction as a function of BChl *g* conversion. (a) Steady-state flavodoxin reduction rate (open circles) and light-induced photobleaching of P_{800} (solid squares) taken at various states of the RC throughout exposure to light and O_2. The predicted total population of primary donors composed of at least one BChl *g*′ molecule (either BChl *g*′/BChl *g*′ or BChl *g*′/Chla_F′ is shown as a dashed red line). (b) Light saturation curves for flavoredoxin reduction in the 0% (black squares and line) and 70% Bchl *g* converted samples (red squares and line). The dotted line depicts the half-saturation values. The inset shows the double reciprocal plot of flavodoxin reduction versus light intensity. The difference in the *y*-intercept for the two samples indicates the decrease in V_{max} upon conversion, whereas the shift in the *x*-intercept indicates an increase in the half saturation value or K_M. (c) Content of primary donor populations BChl *g*′/BChl *g*′, BChl *g*′/Chl a_F′, or Chl a_F′/Chl a_F′ as a function of BChl *g* conversion (see text for details). (d) Difference spectra of as isolated HbRCs (black squares and solid line) and HbRCs with 89% of initial BChl *g* converted to Chl *a* (open circles and dashed line).

special pair increases with conversion (green line). In both cases, the conversion follows a quadratic relationship. In contrast, the concentration of the heterodimeric special pair (BChl *g*′/Chl *a*′) increases to a maximum at 50% conversion and then decreases thereafter (black line). The sum of the concentrations of the (BChl *g*′/BChl *g*′) and (BChl *g*′/Chl *a*′) forms gives the red curve in Figure 4C. Since the activity of the RCs eventually decreases to zero as the conversion nears completion, we can safely assume that the (Chl *a*′/Chl *a*′) form of the special pair is inactive. Hence, the activity should follow the brown curve from Figure 4C if conversion of one of the two chlorophylls is sufficient to render the RC inactive and the red curve if both chlorophylls must be converted. As can be seen in Figure 4A, the red curve fits well the experimental activity data observed for both flavodoxin reduction and P_{800} photobleaching. This suggests that the loss of activity stems exclusively from the fraction of RCs in which both primary donor pigments have been converted (i.e., Chl *a*′/Chl *a*′) (Figure 4C, green line). Consistent with this assessment, when BChl *g* is ~90% converted to Chl *a*, no significant photobleaching is detected, implying that no long-lived charge separated trap is formed at wavelengths characteristic of Chl *a* (670 nm) (Figure 4D).

3.6. Lifetime of the Charge Separation at 80 K. Figure 5 shows transient EPR time traces of P_{800}^{+} collected at 80 K using field modulation detection from which the lifetime of the charge separation can be obtained. In the sample that has not been exposed to O_2 (Figure 5A), the signal decays monoexponentially with a lifetime of 4.2 ± 0.5 ms. Exposure to O_2 and the accompanying conversion of BChl *g* to Chl a_{ox} leads to a decrease in the overall intensity of the signal and the appearance of an additional fast component with a lifetime of 0.3 ± 0.1 ms. The appearance of a kinetic fast component in the backreaction indicates that at least one of the electron transfer cofactors has been altered and it is likely that it occurs in HbRCs in which one of the BChl *g*′ molecules of P_{800} has been converted to Chl *a*′. The relative amplitudes of these two components as a function of the exposure time are shown in Figure 5B. As can be seen, the amplitude of the slow component (red circles) decays with increasing exposure, while the fast component (blue circles) initially increases and then decreases. The sum of the two amplitudes (black circles) decreases. Qualitatively, the 4.2 ms component appears to follow the predicted content of the Bchl *g*′/Bchl *g*′ special pair, and the 0.3 ms component follows the predicted content of the Bchl *g*′/Chl *a*′ special pair. However, the exposure to O_2 and illumination at 80 K also lead to accumulation of a stable *g* = 2 signal probably due to P_{800}^{+}, which is formed when electrons are lost from F_X to residual O_2 in the samples. The amplitude of this signal is plotted in Figure 5C. Because the kinetic phases

DOI: 10.1021/acs.jpcb.5b03339
J. Phys. Chem. B XXXX, XXX, XXX−XXX

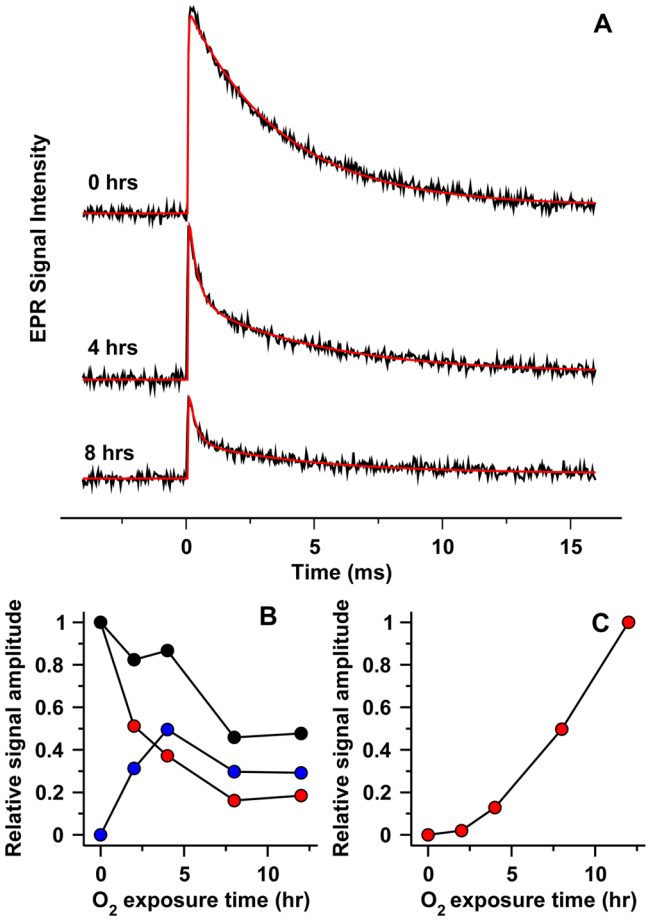

Figure 5. Field-modulation-detected transient EPR studies of the P_{800}^{+} radical after partial conversion of BChl *g*. (A) Charge recombination decay kinetics as a function of oxygen exposure. (B) Amplitudes of the kinetic phases of the charge recombination kinetics. Red circles, 4.2 ms phase; blue circles, 0.3 ms phase; black circles, total amplitude of both phases. (C) Amplitude of stable photoaccumulated P_{800}^{+}.

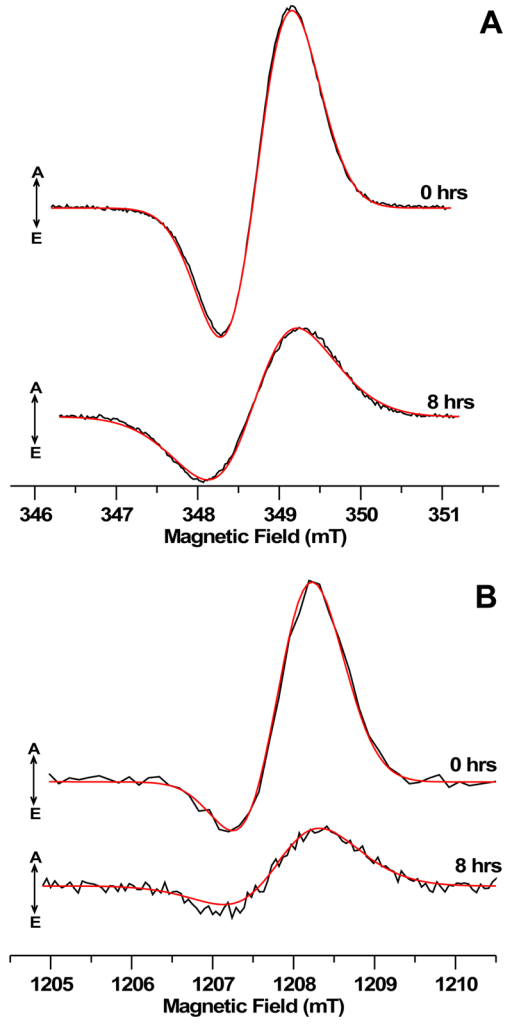

Figure 6. Spin polarized transient EPR spectra of P_{800}^{+} F_X^{-} taken at the X-band (A) and Q-band (B). The black traces are spectra recorded at 80 K after exposure to oxygen for the amount of time indicated next to each spectrum. The red traces are simulations described in the text.

represent the response to single flashes, while the stable P_{800}^{+} signal accumulates with repeated flashes, a quantitative analysis of their amplitudes in terms of the percent conversion of BChl *g* and possible forms of the special pairs in the sample is not feasible.

3.7. Spin Polarized EPR Spectrum of $P_{800}^{+}F_X^{-}$ at 80 K.

The presence of two kinetic phases in the backreaction indicates that the O_2-exposed samples contain a population of functionally active RCs in which one or more of the cofactors have been altered. This raises the question of whether the rate of forward electron transfer to F_X is altered and whether the spectroscopic properties of P_{800}^{+} are changed. Both of these questions can be addressed by transient EPR experiments. Figure 6 shows spin-polarized transient EPR spectra of $P_{800}^{+}F_X^{-}$ taken at 80 K at X-band (A) and Q-band (B). The spectra arise from transitions associated with P_{800}^{+} and show an E/A polarization pattern. The absorptive parts of the spectra are stronger than the emissive parts, indicating that the spin system has net absorptive polarization as a result of singlet−triplet (S−T) mixing in the precursor state $P_{800}^{+}A_0^{-}$. An analytical treatment of sequential radical pairs[29] shows that the polarization can be broken down into three main components. A purely multiplet contribution (equal amounts of emission and absorption) from singlet electron transfer, a net contribution due to S−T mixing during the lifetime of the precursor, and a multiplet contribution to the polarization of only the donor cation due to the influence of inhomogeneous line broadening (e.g., from unresolved hyperfine couplings) on the S−T mixing. The intensity of the net contribution is given by

$$I_{\text{net}} \approx \frac{q_0 b_0}{k^2} \tag{1}$$

where $q_0 = \omega_P - \omega_{A0} = (\beta B_0/\hbar)(g_P - g_{A0})$ is the difference of the precession frequencies of the two spins in the primary radical pair, $b = 2d + J$ is the spin−spin coupling, and k is the rate of electron transfer from A_0^{-} to F_X. The hyperfine contribution is

$$I_h \propto \frac{b_0 D}{k^2} \tag{2}$$

where D is the inhomogeneous line width of the donor.

Using this model, the polarization patterns of anaerobic samples from heliobacteria can be reproduced well[29−31] by taking into account the mixing that occurs during the 600 ps lifetime of the precursor state $P_{800}^{+}A_0^{-}$. The simulated spectra

DOI: 10.1021/acs.jpcb.5b03339
J. Phys. Chem. B XXXX, XXX, XXX−XXX

of the anaerobic sample in Figure 6 (red curves at 0 h exposure) are calculated using the parameters derived from photosystem I as reported previously,[31] except that the line width associated with P_{800}^+ is 0.435 mT instead of the value of 0.40 mT used in the earlier simulations. As can be seen, the absorptive net polarization (difference in intensity of the absorptive and emissive peaks) is much larger in the Q-band spectra (Figure 6B) than in the X-band spectra (Figure 6A), as predicted by eq 1. Upon exposure to oxygen, the intensity of the signal drops but the overall line width increases noticeably and the amount of net polarization relative to the multiplet polarization is significantly less. Because the multiplet contribution associated with hyperfine coupling induced S−T mixing depends on the line width of the donor (eq 2), while the net polarization does not, an increase in the line width leads to an increase in the amplitude of the multiplet polarization relative to the net polarization. On the basis of the biphasic backreaction kinetics and flavodoxin reduction studies, we expect that the spectra of the samples that have been exposed to O_2 arise from a mixture of radical pairs with either (BChl g'/BChl g') or (BChl g'/Chl a_{ox}') as the special pair. If the line width of P_{800}^+ in the (BChl g'/Chl a_{ox}') special pair is taken as 0.60 mT and the relative amounts of the two radical pairs are taken from the ratio of the fast and slow phases in the backreaction, good agreement with the experimental spectra is obtained, as can be seen in the simulations for the sample exposed to oxygen for 8 h shown in Figure 6. From this, we can conclude that the population of HbRCs with fast backreaction kinetics has a special pair with a larger inhomogeneous line width. Such an increase in line width is expected in a heterodimeric special pair due to localization of the unpaired spin density on one of the two chlorophylls. However, other factors such as changes in the T_2 relaxation time and altered matrix hyperfine couplings could also account for the difference in line width. Thus, further experimental data such as ENDOR spectra of P_{800}^+ are needed to determine the origin of the line width change.

3.8. Triplet State Formation at 80 K. Figure 7A shows experimental spin polarized chlorophyll triplet state spectra of the HbRC taken at 80 K and calculated spectra fitted to the experimental ones. In the absence of O_2, an emission/absorption (E/A) pattern ∼60 mT wide triplet state spectrum is observed. The narrow E/A ∼4 mT wide features are from the radical pair $P_{800}^+F_X^-$. The polarization pattern of the triplet spectrum indicates that the triplet state is formed by intersystem crossing, and the values of the zero-field-splitting parameters $D = 2.15 \times 10^{-2}$ cm^{-1} and $E = 7.2 \times 10^{-3}$ cm^{-1} are consistent with those reported previously[32,33] for the triplet state of BChl g. Upon exposure to O_2 for 12 h in the dark, additional features appear in the spectrum. The additional contribution is consistent with the triplet state of a Chl a species with $D = 2.71 \times 10^{-2}$ cm^{-1} and $E = 3.3 \times 10^{-3}$ cm^{-1} and a polarization pattern that is determined by intersystem crossing. Very weak features in the wings of the spectrum suggest that there may also be a small contribution from carotenoid triplet states as well. The spectra of all of the O_2-exposed samples can be simulated as a weighted sum of the BChl g and Chl a_F spectra shown at the bottom of Figure 7A. The amplitudes of these contributions relative to the amplitude of the triplet spectrum in the anaerobic sample are plotted in Figure 7B. As can be seen, the intensities of both contributions increase with increasing exposure time. These results suggest that the gradual conversion of BChl g to Chl a_F has two effects.

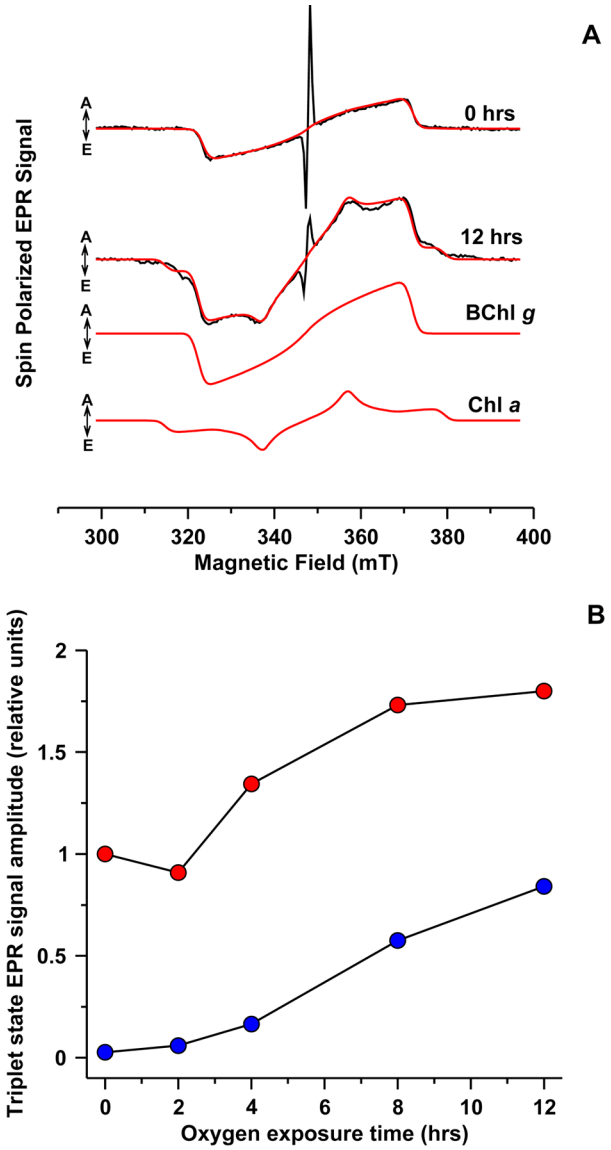

Figure 7. (A) Spin polarized triplet state spectra. The upper two spectra are experimental (black) and simulated (red) spectra before and after exposure to oxygen. The narrow emission/absorption pattern at the center of the spectra is due to the radical pair $P_{800}^+F_X^-$ The lower two spectra in panel A are simulations of spectra of the triplet states of BChl g and Chl a. In both cases, the triplet state is formed by intersystem crossing. (B) Relative amplitudes of the BChl g and Chl a contributions to the triplet spectra. The red circles are the BChl g contribution, and the blue circles are the Chl a contribution.

The appearance of a Chl a_F triplet spectrum implies that, at 80 K, the converted molecules are unable to transfer their excitation energy. The increase in the amplitude of the BChl g triplet signal suggests that some of the antenna BChl g molecules that would otherwise transfer their excitation energy to neighboring chlorophyll molecules are unable to do so. However, it is unclear whether this is the result of the conversion of neighboring BChl g molecules or the presence of closed RCs in which P_{800} has been trapped in an oxidized state.

4. DISCUSSION

The conversion of BChl g to Chl a_{ox} in purified RCs from *H. modesticaldum* is a function of light, temperature, and O_2. In the presence of O_2, we observe an immediate conversion of BChl g

DOI: 10.1021/acs.jpcb.5b03339
J. Phys. Chem. B XXXX, XXX, XXX−XXX

to Chl a_{ox} in the light, but there is a distinct lag in the absence of light. The length of the lag as well as the conversion process is temperature dependent. The Arrhenius behavior of the dark conversion process indicates that the HbRC is increasingly stable as the temperature is lowered, which is of practical importance for the handling of these preparations. At 9 °C, the duration of the slow kinetic phase before the relatively sharp transition to the fast conversion of BChl *g* to Chl a_{ox} is about 12 h. When the sample is kept on ice, the duration of the slow kinetic phase is on the order of days. Increasing the temperature to 32 °C results in a rapid conversion of over 90% of the BChl *g* to Chl a_{ox} within 10 min. Hence, the conversion of BChl *g* to Chl a_{ox} can be precisely controlled with the use of light, oxygen, and temperature. Significantly, at 0 °C and in darkness, the conversion was so slow that we were able to handle the RCs for 12 h in weak green light in air without detectable conversion of BChl *g*. We can surmise that the activation energies observed for the conversion of BChl *g* reflect a rate-limiting barrier. The fact that there is a lag phase suggests a multistep mechanism involving an intermediate that must accumulate to a critical concentration before the conversion can occur to any large extent. This is supported by the observation that the conversion is strongly inhibited by menadione, which implies that it hinders the accumulation of the intermediate. The fact that isosbestic points are observed in the absorption spectra implies that the proposed intermediate does not absorb in the UV−vis region. It is likely that several different reactions occur either simultaneously or in sequence, since several different oxidized forms of Chl a_F are observed. A small amount of genuine Chl a_F was also found, but it was likely formed by exposure to acid in the post-treatment step prior to HPLC analysis. The mechanism by which the 1,3-hydride shift occurs is not known; however, it is thermally forbidden according to the Woodward−Hoffmann rules.[34] Thus, in solution, it requires acid[24] and *in vivo* O_2 is needed.[23] Our data show that it occurs in combination with oxidative addition of hydroxyl groups to the chlorophyll and that subsequent dehydration of the dihydroxyl adduct may also occur.

The data also indicate that, as BChl *g* is converted to Chl a_{ox}, the homodimeric BChl *g*′/BChl *g*′ special pair is converted at the same rate as the bulk BChl *g* cofactors, which implies the presence of an intermediate heterodimeric Chl *a*′/BChl *g*′ special pair prior to the final homodimeric Chl *a*′/Chl *a*′ special pair. The flavodoxin reduction data, the appearance of biphasic backreaction kinetics, and the changes in the line width of the TREPR spectra all suggest that the heterodimeric special pair is functionally active. The significance of this finding is that it implies that three different forms of the special pair with different electron transfer kinetics can be generated and studied within the same protein matrix. The flavodoxin assay indicates that HbRCs that contain BChl *g*′/BChl *g*′ and Chl *a*′/BChl *g*′ special pairs are functional in carrying out electron transfer, whereas HbRCs that contain the Chl *a*′/Chl *a*′ special pair are not. This implies that the conversion does not completely impair the function of the HbRCs until both BChl *g*′ molecules of the special pair have been converted.

Using a model in which only conversion of the special pair chlorophylls is considered and it is assumed that only Chl *a*′/Chl *a*′ special pairs are inactive, it can be shown that, as BChl *g*′ is increasingly converted to Chl a_F′, the ratio of Chl *a*′/BChl *g*′ special pairs to BChl *g*′/BChl *g*′ special pairs increases; however, this process occurs at the expense of total functional RCs. For example, at 70% conversion of BChl *g*, the functional RCs consist of a 4.2:1 ratio of Chl *a*′/BChl *g*′ special pairs relative to BChl *g*′/BChl *g*′ special pairs. Their sum represents 52% of the number of initially functional BChl *g*′/BChl *g*′ special pairs. It is therefore statistically possible to obtain a majority population of HbRCs with heterodimeric special pairs by selective pigment oxidation. The model, which fits the experimental data, assumes that the quantum yield of charge separation is the same in HbRCs containing BChl *g*′/BChl *g*′ and Chl *a*′/BChl *g*′ special pairs. This is in contrast to RCs of a *Rhodobacter capsulatus* mutant, which incorporate a BPh/BChl heterodimer as the primary donor and show a roughly 50% reduction in the quantum yield of electron transfer.[35] However, the latter are type II RCs with unidirectional electron transfer, while HbRCs are homodimeric type I RCs, in which the electron transfer is expected to be bidirectional.

The samples that are expected to contain a majority of Chl *a*′/BChl *g*′ special pairs also show the largest relative amounts of the fast backreaction phase and the species with a broader P_{800}^+ line width. All of these data are consistent with the presence of RCs that contain a population of functional Chl *a*′/BChl *g*′ special pairs. In contrast to purple bacterial reaction centers, excitonic coupling does not cause strong shifts of the chorophyll absorption bands in HbRCs. Hence, bleaching of the proposed Chl *a*′/BChl *g*′ special pairs is expected to occur either at the absorbance wavelength of BChl *g* (800 nm) or Chl a_F (670 nm). The data in Figure 4 all point toward bleaching occurring only at 800 nm. However, this evidence is mostly indirect and further studies are needed to determine more conclusively whether heterodimer special pairs are present and where they absorb. Irrespective of the details of the conversion, the fact that the spin polarization patterns indicate that the rate of electron transfer from A_0^- to F_X is unaffected and the lack of evidence for triplet recombination of the primary radical pair $P_{800}^+A_0^-$ suggests that the inactivation is the result of loss of the primary charge separation.

These findings may have physiological implications for the fitness and survivability of *H. modesticaldum* in its native environment. Heliobacteria are soil-dwelling organisms that exist primarily as terrestrial phototrophs rather than aquatic phototrophs and are thought to have evolved in a mutualistic relationship with plants, particularly rice.[36] They are strict photoheterotrophs; hence, they use light as an energy source but rely on fixed carbon in the form of pyruvate, lactate, and/or acetate supplied by a plant.[37] In return, they fix nitrogen and complete the symbiotic relationship by supplying the plant with glutamate. The HbRC uses light to generate ATP by cyclic electron transfer, thereby supplying the energetic requirements required by nitrogen fixation.[38] The environment of a germinating rice patty provides the anoxic conditions for BChl *g* to be retained in a stable form in the presence of light. However, were the Heliobacteria to become transiently exposed to O_2, there would be a rapid conversion of BChl *g* to Chl a_{ox}. *H. modesticaldum* is, moreover, a mild thermophile, growing optimally at 48 °C; hence, the conversion would be especially rapid. However, given that the BChl *g*′/BChl *g*′ and Chl *a*′/BChl *g*′ special pairs are both functional, the organism would be able to withstand 50% conversion of Bchl *g* while still retaining 75% functional RCs. This might provide enough of an energetic margin for the organism to repair the damage and survive in what would otherwise be an inhospitable environment.

DOI: 10.1021/acs.jpcb.5b03339
J. Phys. Chem. B XXXX, XXX, XXX−XXX

AUTHOR INFORMATION

Corresponding Authors

*E-mail: hhou@alasu.edu.
*E-mail: jhg5@psu.edu.
*E-mail: avde@brocku.ca.

Notes

The authors declare no competing financial interest.
[%]Bryan Ferlez and Weibing Dong should be considered co-first authors.

ACKNOWLEDGMENTS

This work was supported by a Discovery Grant from the Natural Science and Engineering Research Council of Canada to A.v.d.E. and a grant from the U.S. Department of Energy, Chemical Science, Geoscience, & Biosciences Division (DE-FG02-98ER20314) to J.H.G. and K.R. H.J.M.H. thanks Alabama State University for financial support. We thank Nicholas Lanz and Dr. Squire Booker for use of their LC-MS instrument and technical assistance in collecting and processing the data.

ABBREVIATIONS

HbRC, Heliobacterium reaction center; BChl *g*, bacteriochlorophyll *g*; Chl *a*, chlorophyll *a*

REFERENCES

(1) Gest, H.; Favinger, J. *Heliobacterium chlorum*, an Anoxygenic Brownish-Green Photosynthetic Bacterium Containing a "New" Form of Bacteriochlorophyll. *Arch. Microbiol.* **1983**, *136*, 11−16.

(2) Heinnickel, M.; Golbeck, J. H. Heliobacterial Photosynthesis. *Photosynth. Res.* **2007**, *92*, 35−53.

(3) Madigan, M. T. Heliobacteriaceae. In *Bergey's Manual of Systematic Bacteriology*, 2nd ed.; Boone, E., Castenholz, R. W., Carrity, G. M., Eds.; Springer-Verlag: New York, 2001; Vol. *1*, pp 625−630.

(4) Heinnickel, M.; Agalarov, R.; Svensen, N.; Krebs, C.; Golbeck, J. H. Identification of Fx in the Heliobacterial Reaction Center as a [4Fe-4S] Cluster with an S = 3/2 Ground Spin State. *Biochemistry* **2006**, *45*, 6756−6764.

(5) Sarrou, I.; Khan, Z.; Cowgill, J.; Lin, S.; Brune, D.; Romberger, S.; Golbeck, J. H.; Redding, K. E. Purification of the Photosynthetic Reaction Center from *Heliobacterium modesticaldum*. *Photosynth. Res.* **2012**, *111*, 291−302.

(6) Neerken, S.; Amesz, J. The Antenna Reaction Center Complex of Heliobacteria: Composition, Energy Conversion and Electron Transfer. *Biochim. Biophys. Acta* **2001**, *1507*, 278−290.

(7) Takaichi, S.; Inoue, K.; Akaike, M.; Kobayashi, M.; Oh-oka, H.; Madigan, M. T. The Major Carotenoid in All Known Species of Heliobacteria Is the C30 Carotenoid 4,4′-Diaponeurosporene, Not Neurosporene. *Arch. Microbiol.* **1997**, *168*, 277−281.

(8) Prince, R. C.; Gest, H.; Blankenship, R. E. Thermodynamic Properties of the Photochemical-Reaction Center of *Heliobacterium chlorum*. *Biochim. Biophys. Acta* **1985**, *810*, 377−384.

(9) van de Meent, E. J.; Kobayashi, M.; Erkelens, C.; van Veelen, P. A.; Amesz, J.; Watanabe, T. Indentification of 8^1-Hydroxychlorophyll *a* as a Functional Reaction Center Pigment in Heliobacteria. *Biochim. Biophys. Acta* **1991**, *1058*, 356−362.

(10) Amesz, J. The Heliobacteria, a New Group of Photosynthetic Bacteria. *J. Photochem. Photobiol., B* **1995**, *30*, 89−96.

(11) Romberger, S. P.; Golbeck, J. H. The F-X Iron-Sulfur Cluster Serves as the Terminal Bound Electron Acceptor in Heliobacterial Reaction Centers. *Photosynth. Res.* **2012**, *111*, 285−290.

(12) Hiraishi, A. Occurrence of Menaquinone as the Sole Isoprenoid Quinone in the Photosynthetic Bacterium *Heliobacterium chlorum*. *Arch. Microbiol.* **1989**, *151*, 378−379.

(13) Lin, S.; Chiou, H. C.; Kleinherenbrink, F. A.; Blankenship, R. E. Time-Resolved Spectroscopy of Energy and Electron Transfer Processes in the Photosynthetic Bacterium *Heliobacillus mobilis*. *Biophys. J.* **1994**, *66*, 437−445.

(14) Nuijs, A. M.; Dorssen, R. J. v.; Duysens, L. N. M.; Amesz, J. Excited States and Primary Photochemical Reactions in the Photosynthetic Bacterium *Heliobacterium chlorum*. *Proc. Natl. Acad. Sci. U.S.A.* **1985**, *82*, 6865−6868.

(15) Van Kan, P. J.; Aartsma, T. J.; Amesz, J. Primary Photosynthetic Processes in *Heliobacterium chlorum* at 15 K. *Photosynth. Res.* **1989**, *22*, 61−68.

(16) Lin, S.; Chiou, H.-C.; Blankenship, R. E. Secondary Electron Transfer Processes in Membranes of *Heliobacillus mobilis*. *Biochemistry* **1995**, *34*, 12761−12767.

(17) Brettel, K.; Leibl, W.; Liebl, U. Electron Transfer in the Heliobacterial Reaction Center: Evidence against a Quinone-Type Electron Acceptor Functioning Analogous to A1 in Photosystem I. *Biochim. Biophys. Acta* **1998**, *1363*, 175−181.

(18) Kleinherenbrink, F. A. M.; Ikegami, I.; Hiraishi, A.; Otte, S. C. M.; Amesz, J. Electron Transfer in Menaquinone-Depleted Membranes of *Heliobacterium chlorum*. *Biochim. Biophys. Acta* **1993**, *1142*, 69−73.

(19) Van der Est, A.; Hager-Braun, C.; Leibl, W.; Hauska, G.; Stehlik, D. Transient Electron Paramagnetic Resonance Spectroscopy on Green-Sulfur Bacteria and Heliobacteria at Two Microwave Frequencies. *Biochim. Biophys. Acta* **1998**, *1409*, 87−98.

(20) Muhiuddin, I. P.; Rigby, S. E.; Evans, M. C.; Amesz, J.; Heathcote, P. Endor and Special Triple Resonance Spectroscopy of Photoaccumulated Semiquinone Electron Acceptors in the Reaction Centers of Green Sulfur Bacteria and Heliobacteria. *Biochemistry* **1999**, *38*, 7159−7167.

(21) Brok, M.; Vasmel, H.; Horikx, J. T.; Hoff, A. J. Electron Transport Components of *Heliobacterium chlorum* Investigated by Epr Spectroscopy at 9 and 35 GHz. *FEBS Lett.* **1986**, *194*, 322−326.

(22) Miyamoto, R.; Mino, H.; Kondo, T.; Itoh, S.; Oh-Oka, H. An Electron Spin-Polarized Signal of the P800+ A1(Q)− State in the Homodimeric Reaction Center Core Complex of *Heliobacterium modesticaldum*. *Biochemistry* **2008**, *47*, 4386−4393.

(23) Beer-Romero, P.; Favinger, J. L.; Gest, H. Distinctive Properties of Baxilliform Photosynthetic Heliobacteria. *FEMS Microbiol. Lett.* **1988**, *49*, 451−454.

(24) Kobayashi, M.; Hamano, T.; Akiyama, M.; Watanabe, T.; Inoue, K.; Oh-oka, H.; Amesz, J.; Yamamura, M.; Kise, H. Light-Independent Isomerization of Bacteriochlorophyll *g* to Chlorophyll *a* Catalyzed by Weak Acid *in Vitro*. *Anal. Chim. Acta* **1998**, *365*, 199−203.

(25) Brockmann, H., Jr.; Lipinski, A. Bacteriochlorophyll *G*. A New Bacteriochlorophyll from *Heliobacterium chlorum*. *Arch. Microbiol.* **1983**, *136*, 17−19.

(26) Michalski, T.; Hunt, J.; Bowman, M.; Smith, U.; Bardeen, K.; Gest, H.; Norris, J.; Katz, J. Bacteriopheophytin *g*: Properties and Some Speculations on a Possible Primary Role for Bacteriochlorophylls *b* and *g* in the Biosynthesis of Chlorophylls. *Proc. Natl. Acad. Sci. U.S.A.* **1987**, *84*, 2570−2574.

(27) Thamarath, S. S.; Alia, A.; Daviso, E.; Mance, D.; Golbeck, J. H.; Matysik, J. Whole Cell Nuclear Magnetic Resonance Characterization of Two Photochemically Active States of the Photosynthetic Reaction Center in Heliobacteria. *Biochemistry* **2012**, *51*, 5763−5773.

(28) Stevenson, A. K.; Kimble, L. K.; Woese, C. R.; Madigan, M. T. Characterization of New Phototrophic Heliobacteria and Their Habitats. *Photosynth. Res.* **1997**, *53*, 1−12.

(29) Kandrashkin, Y. E.; Salikhov, K. M.; van der Est, A.; Stehlik, D. Electron Spin Polarization in Consecutive Spin-Correlated Radical Pairs: Application to Short-Lived and Long-Lived Precursors in Type 1 Photosynthetic Reaction Centres. *Appl. Magn. Reson.* **1998**, *15*, 417−447.

(30) Kandrashkin, Y. E.; van der Est, A. Time-Resolved Epr Spectroscopy of Photosynthetic Reaction Centers: From Theory to Experiment. *Appl. Magn. Reson.* **2007**, *31*, 105−122.

DOI: 10.1021/acs.jpcb.5b03339
J. Phys. Chem. B XXXX, XXX, XXX−XXX

(31) Kandrashkin, Y. E.; Vollmann, W.; Stehlik, D.; Salikhov, K.; Van der Est, A. The Magnetic Field Dependence of the Electron Spin Polarization in Consecutive Spin Correlated Radical Pairs in Type I Photosynthetic Reaction Centres. *Mol. Phys.* **2002**, *100*, 1431−1443.
(32) Vrieze, J.; Hoff, A. J. The Orientation of the Triplet Axes with Respect to the Optical Transition Moments in (Bacterio) Chlorophylls. *Chem. Phys. Lett.* **1995**, *237*, 493−501.
(33) Vrieze, J.; van de Meent, E. J.; Hoff, A. J. Triplet Properties and Interactions of the Primary Electron Donor and Antenna Chromophores in Membranes of *Heliobacterium chlorum*, Studied with Admr Spectroscopy. *Biochemistry* **1998**, *37*, 14900−14909.
(34) Woodward, R. B.; Hoffmann, R. Selection Rules for Sigmatropic Reactions. *J. Am. Chem. Soc.* **1965**, *87*, 2511−2513.
(35) Kirmaier, C.; Holten, D.; Bylina, E. J.; Youvan, D. C. Electron-Transfer in a Genetically Modified Bacterial Reaction Center Containing a Heterodimer. *Proc. Natl. Acad. Sci. U.S.A.* **1988**, *85*, 7562−7566.
(36) Asao, M.; Madigan, M. T. Taxonomy, Phylogeny, and Ecology of the Heliobacteria. *Photosynth. Res.* **2010**, *104*, 103−111.
(37) Madigan, M. T. The Family Heliobacteriaceae. In *The Prokaryotes*, 4th ed.; Dworkin, M., Falkow, M. S., Rosenberg, E., Scheifer, K.-H., Stackebrandt, E., Eds.; Springer: New York, 2006; pp 951−964.
(38) Madigan, M. T.; Ormerod, J. G., Taxonomy, Physiology, and Ecology of Heliobacteria. In *Anoxygenic Photosynthetic Bacteria*; Blankenship, R. E., Madigan, M. T., Bauer, C. E., Eds.; Kluwer Academic Publishers: Dordrecht, The Netherlands, 1995; pp 17−30.

DOI: 10.1021/acs.jpcb.5b03339
J. Phys. Chem. B XXXX, XXX, XXX−XXX